**Proceedings of the 17th World Congress**
**The International Federation of Automatic Control**
**Seoul, Korea, July 6-11, 2008**

# Vibration Damping of a Flexible Car Body Structure Using Piezo-Stack Actuators ⋆

**Martin Kozek** * **Christian Benatzky** * **Alexander Schirrer** *
**Anton Stribersky** **

* *Vienna University of Technology, 1040 Vienna, Austria (Tel: +43-1-58801-32812; e-mail: kozek@impa.tuwien.ac.at).*
** *Siemens Transportation Systems GmbH & Co KG, Mass Transit, 1110 Vienna, Austria (e-mail: anton.stribersky@siemens.com)*

**Abstract:** In this work piezo-stack actuators mounted in consoles are utilized to actively dampen vibrations of a flexible car body structure by introducing bending moments. Using an example of a heavy metro vehicle the complete design for the active vibration damping system is presented. Both analytical modeling and a system identification of the vehicle are described, issues of modal representation and model reduction are covered, and a robust controller design is motivated and explained. The excellent performance of the proposed method is documented by both experimental results from a scaled model and an extensive co-simulation of the overall system.

Keywords: rail traffic; vibration damping; active control; robust control; vehicles.

## 1. INTRODUCTION

One of the many design aspects of modern railway vehicles is to ensure a good ride quality meaning the reduction of the vibration amplitudes of the car body. This is usually achieved by a careful design of the secondary suspension. Additionally, active control schemes can be employed to generate an active or semi-active secondary suspension system (Foo and Goodall [2000], Stribersky et al. [1998]).

A novel method for vibration reduction is the application of an active control system to attenuate the elastic vibrations of the railway car body. Both passive (Hansson et al. [2004]) and active control schemes (Kamada et al. [2005], Schandl et al. [2007]) have already been proposed. The safety of the vehicle against derailment will not be affected, and retrofitting of existing railway vehicles becomes possible. This approach is especially useful in the design of extremely light-weight railway vehicles. In this case properties such as stiffness and structural damping need not be provided by the structure itself but can be generated by means of the mechatronic damping system.

Due to the size, mass, and stiffness of the structure considerable moments have to be applied by the actuator. For this reason piezo-stack actuators mounted in consoles are proposed which are capable of introducing the necessary moments. The purpose of this paper is to illustrate the design steps of such an active vibration control system and to highlight the performance of this concept. Simulation results for a heavy metro vehicle and experimental results from a scaled model shown in Fig. 1 (Kozek et al. [2006]) demonstrate the potential of the approach. However, the feasibility of a full-scale implementation is still not proven, and further research has to be conducted for that purpose.

⋆ This work was financially supported by the Austrian Federal Ministry of Transport, Innovation and Technology under the FFG project number 809091-KA/HN and Siemens Transportation Systems.


Fig. 1. Experimental setup of a scaled railway car body

In the remainder of this paper a description of the system and the active control scheme is given. Since the finite-element (FE) model always differs from the real vehicle an identification procedure is outlined in the following section and results for the scaled experiment are given. Then a short background on robust control design and the controller design is presented, some considerations on currently available piezo-stack actuators are included, and the resulting performance of the proposed control concept is demonstrated in an extensive co-simulation. The paper is concluded by a discussion and an outlook.

## 2. SYSTEM DESCRIPTION

The dynamics of the bogie elements are described by coupled rigid bodies and for the flexible car body an FE-model is utilized. In Fig. 2 the master nodes of the FE-model of the flexible car body together with the rigid bogie parts are shown. The elastic deformations of the car body are given by a modal representation which assumes that elastic deformations can be represented by a finite sum of spatial shape functions $\phi_i$, each weighted by a temporal function $q(t)$, the so-called modal coordinates. To incorporate local

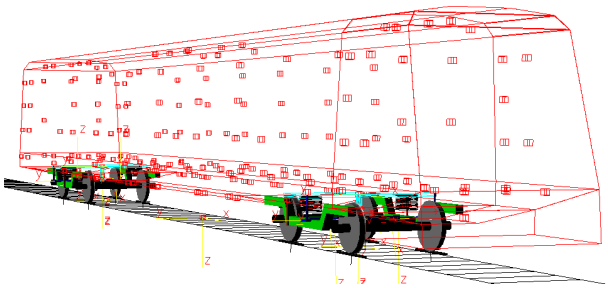

Fig. 2. The FE model of a flexible car body coupled to bogies, modeled by interacting rigid bodies

deformations additional shape functions like static modes are used. In order to overcome the associated problems of finding correct boundary conditions frequency response modes (FRM) are used instead. This concept uses dynamic harmonic forces acting at the location of the actuator attachment points to obtain the frequency response. For each actuator a frequency response mode is calculated and finally a transformation is performed to decouple the FRMs from each other, the elastic modes, and the rigid body modes (Dietz [1999]).

The first 3 eigenfrequencies and eigenmodes of the elastic car body are displayed in Fig. 3. For a given heavy

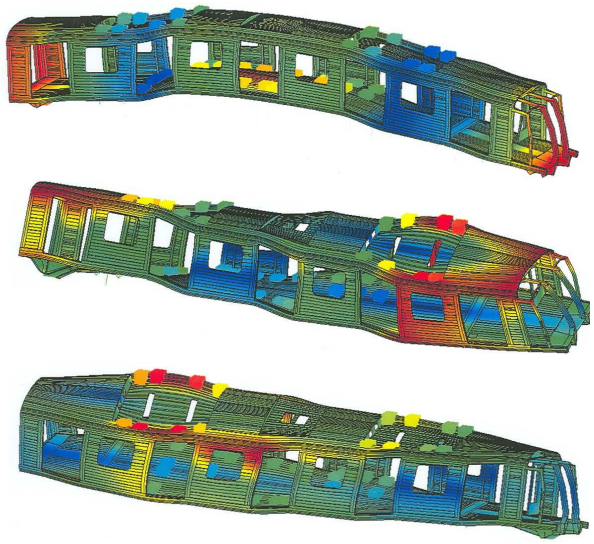

Fig. 3. The first 3 modes of an elastic car body

metro vehicle the elastic deformations of the car body are modeled by 17 eigenmodes with eigenfrequencies in the frequency range from 7 Hz up to approximately 25 Hz and as many FRMs as actuators. The eigenfrequencies of the FRM range from approximately 150 Hz to 700 Hz which is necessary to accurately describe highly localized deformations (Benatzky and Kozek [2005]).

An example for positioning of the actuators and sensors is shown in Fig. 4, and the principle after which the actuators work is shown in Fig. 5. Several criteria for optimal actuator/sensor placement are available (e.g. Gawronski [1997]), and in general the positions with strongest local deformations will result (compare Fig. 3 and Fig. 4). The actuators are assumed to be linear which means that a force generated by the actuator is proportional to

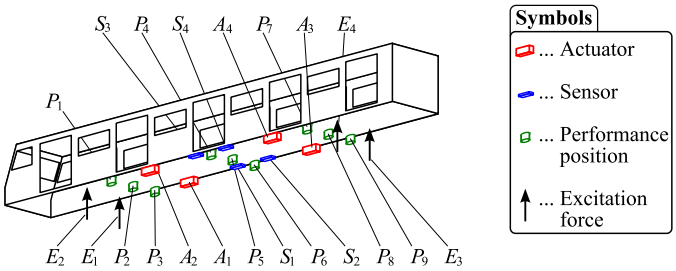


Fig. 4. Actuator/sensor configuration for a car body

the voltage computed by the controller. The simulations presented in section 8 have shown that this assumption holds for commercially available piezo-stacks (blocking force $F_{\mathrm{B}} = 50$ kN, travel $\triangle w = 0.2$ mm, length $l = 294$ mm, and diameter $d = 45$ mm). These actuators proved to be sufficient for achieving good performance in the investigated metro vehicle car body. A more detailed discussion on actuator characteristics can be found in section 7.

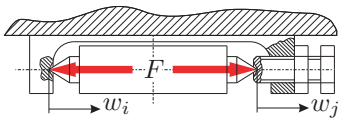


Fig. 5. Piezo-stack actuator mounted in console

## 3. ANALYTICAL MODELING

Only the elastic modes of the car body can be influenced by actuator forces. Therefore, for controller design purposes only a model of the elastic modes of the car body is necessary. These equations of motion are given by the following system of differential equations of order $n$:

$$\boldsymbol{M}\ddot{\boldsymbol{w}} + \boldsymbol{L}\dot{\boldsymbol{w}} + \boldsymbol{K}\boldsymbol{w} = \boldsymbol{f}(t). \tag{1}$$

Here $\boldsymbol{M}$ is the $(n \times n)$ mass matrix, $\boldsymbol{L}$ is the $(n \times n)$ damping matrix, $\boldsymbol{K}$ is the $(n \times n)$ stiffness matrix, and $\boldsymbol{f}(t)$ is the $(n \times 1)$ vector of generalized excitation forces containing excitation as well as control forces. A transformation is defined by replacing the $(n \times 1)$ vector of generalized coordinates $\boldsymbol{w}(t)$ with

$$\boldsymbol{w}(t) = \boldsymbol{\Phi}\boldsymbol{q}(t) = \sum_{j=1}^{n} \boldsymbol{\phi}_j q_j(t), \tag{2}$$

where

$$\boldsymbol{\Phi} = [\boldsymbol{\phi}_1, \boldsymbol{\phi}_2, \ldots, \boldsymbol{\phi}_n]^T$$

is the matrix of eigenvectors of (1). Inserting (2) into (1) and left-multiplying by $\boldsymbol{\Phi}^T$, one obtains a diagonal system in modal coordinates

$$\ddot{\boldsymbol{q}} + 2\boldsymbol{\zeta}\boldsymbol{\Omega}\dot{\boldsymbol{q}} + \boldsymbol{\Omega}^2\boldsymbol{q} = \boldsymbol{\mu}^{-1}\boldsymbol{\Phi}^T\boldsymbol{f}(t), \tag{3}$$

where $\boldsymbol{\mu}$ is the $(n \times n)$ matrix of modal masses, $\boldsymbol{\zeta}$ is the $(n \times n)$ matrix of modal dampings and $\boldsymbol{\Omega}$ is the $(n \times n)$ matrix of undamped eigenfrequencies. Definition of

$$\boldsymbol{x} = [\boldsymbol{q}, \dot{\boldsymbol{q}}]^T \tag{4}$$

leads to the state space system equation

$$\dot{\boldsymbol{x}} = \boldsymbol{A}\boldsymbol{x} + \boldsymbol{B}_1\boldsymbol{d} + \boldsymbol{B}_2\boldsymbol{u} \tag{5}$$

and the output equation

$$\boldsymbol{y} = \boldsymbol{C}_2\boldsymbol{x}, \tag{6}$$

which together form the state space description of (3). In (5) and (6) $\boldsymbol{A}$ is the $(2n \times 2n)$ system matrix, $\boldsymbol{B}_1$ is the $(2n \times l)$ disturbance input matrix, $\boldsymbol{B}_2$ is the $(2n \times m)$ input matrix, $\boldsymbol{C}_2$ is the $(p \times 2n)$ measurement output matrix, $\boldsymbol{x}$ is the $(2n \times 1)$ state vector, $\boldsymbol{u}$ is the $(m \times 1)$ vector of control signals, $\boldsymbol{d}$ is the $(l \times 1)$ vector of disturbances (excitation of the car body from secondary suspension) and $\boldsymbol{y}$ is the $(p \times 1)$ vector of controlled variables. The controlled variables may consist of measured outputs as well as of performance variables.

If one actuator is used, forces are acting in the directions $w_i$ and $w_j$ according to Fig. 5, and if only one excitation force is acting on the structure in the direction $w_l$, the disturbance input matrix $\boldsymbol{B}_1$ and the input matrix $\boldsymbol{B}_2$ are

$$\boldsymbol{B}_1 = \begin{bmatrix} 0 \\ \vdots \\ 0 \\ \phi_1(w_l) \\ \vdots \\ \phi_n(w_l) \end{bmatrix}, \quad \boldsymbol{B}_2 = \begin{bmatrix} 0 \\ \vdots \\ 0 \\ \phi_1(w_j) - \phi_1(w_i) \\ \vdots \\ \phi_n(w_j) - \phi_n(w_i) \end{bmatrix}. \tag{7}$$

In (7) $\phi_m(w_j)$ is the component of $\boldsymbol{\phi}_m$ in direction of $w_j$. When the sensors are collocated with the actuators (Preumont [1997]), the output matrix $\boldsymbol{C}_2$ is proportional to the input matrix $\boldsymbol{B}_2$

$$\boldsymbol{C}_2 = \frac{1}{l_s}\boldsymbol{B}_2^T, \tag{8}$$

where $l_s$ is the distance between the nodes $w_i$ and $w_j$ in the unstrained state.

Equivalent transfer function descriptions for (5) and (6) are given by

$$\boldsymbol{G}_{su} = \boldsymbol{C}_2(s\boldsymbol{I} - \boldsymbol{A})^{-1}\boldsymbol{B}_2 \tag{9}$$

for the open loop transfer function from actuator action to the outputs and

$$\boldsymbol{G}_{sd} = \boldsymbol{C}_2(s\boldsymbol{I} - \boldsymbol{A})^{-1}\boldsymbol{B}_1 \tag{10}$$

for the open loop action of the disturbances on the outputs.

## 4. SYSTEM IDENTIFICATION

Considerable differences may occur between the FE design model and the manufactured vehicle regarding the predicted eigenfrequencies as well as the assumed damping coefficients. A proper identification procedure is therefore needed to obtain an accurate mathematical model for controller design. This approach has been experimentally validated using a scaled model of a car body, for which such a mathematical model has been identified.

### *4.1 State space representation*

Augmenting the output equation (6) with a $q \times 1$ performance vector $\boldsymbol{z}$ (typically vertical accelerations at various positions), the overall representation becomes

$$\begin{bmatrix} \dot{\boldsymbol{x}} \\ \boldsymbol{z} \\ \boldsymbol{y} \end{bmatrix} = \begin{bmatrix} \boldsymbol{A} & \boldsymbol{B}_1 & \boldsymbol{B}_2 \\ \boldsymbol{C}_1 & \boldsymbol{D}_{11} & \boldsymbol{D}_{12} \\ \boldsymbol{C}_2 & \boldsymbol{D}_{21} & \boldsymbol{D}_{22} \end{bmatrix} \begin{bmatrix} \boldsymbol{x} \\ \boldsymbol{d} \\ \boldsymbol{u} \end{bmatrix}. \tag{11}$$

Here $\boldsymbol{C}_1$ is the $q \times n$ performance output matrix and $\boldsymbol{D}_{11}$, $\boldsymbol{D}_{12}$, $\boldsymbol{D}_{21}$, and $\boldsymbol{D}_{22}$ are the feed-through matrices. The explicit notation of performance variables $\boldsymbol{z}$ is reasonable since only strains are measured but the accelerations are used to quantify performance. Furthermore, this system structure is well suited for a robust controller design (see section 6).

### *4.2 Identification procedure*

The MIMO system (11) is identified from the scaled car body experiment (Kozek et al. [2006]) utilizing the `n4sid`-algorithm as implemented in MATLAB. In the experimental setup, measured secondary suspension forces for the identification of disturbance transfer functions have to be applied to the car body structure (Benatzky and Kozek [2007]). For an actual rail vehicle these measurements can be performed during test runs.

A suitable sampling time for measurements was found to be $T_\mathrm{s} = 0.001$s. Applying the data sets to the `n4sid`-algorithm, a model of order 200 is identified and then transformed to the modal representation (11). This model is referred to as "full model". It is then subject to a preliminary reduction since eigenfrequencies from local vibration modes can lie very close to global vibration modes. Therefore, these additional poles, which are usually less controllable and observable than the global modes, first have to be removed. Finally, a balanced reduction is performed which retains only 3 eigenmodes. Table 1

Table 1. Natural frequencies $\omega_n$ and damping coefficients $\zeta$ for a scaled laboratory model

| Eigenmode | $\omega_\mathrm{n}$ [Hz] | $\zeta$ [1] |
|---|---|---|
| First vertical bending mode | 65.66 | 0.0037 |
| First torsional mode | 73.91 | 0.0043 |

exemplarily shows the eigenfrequencies $\omega_\mathrm{n}$ and the modal damping coefficients $\zeta$ for the modes of the scaled laboratory car body (eigenfrequencies are roughly 8 times higher than for the actual vehicle). In Fig. 6 the identified transfer functions $G_{y_1u_1}$ of this experiment for the "full model" and the "balanced reduced model" are compared with an empirical non-parametric transfer function estimate $T_{y_1u_1}$. The identified transfer function $G_{y_1u_1}$ shows an excellent match with the transfer function estimate $T_{y_1u_1}$.

## 5. BACKGROUND ON $\mu$-SYNTHESIS

### *5.1 Structure of robust control systems*

The open loop system $\boldsymbol{P}$ with controller $\boldsymbol{K}$ and uncertainties $\boldsymbol{\Delta}$ is shown in Fig. 7, left. The output vector $\boldsymbol{z}$ contains the performance variables, while the vector of measurements $\boldsymbol{y}$ is only used for feedback control. Therefore, this system structure is ideal for the current control problem. Using lower and upper fractional transformations, $\boldsymbol{K}$ is absorbed into $\boldsymbol{P}$ forming $\boldsymbol{M}$, and consequently $\boldsymbol{\Delta}$ into $\boldsymbol{M}$ yielding $\boldsymbol{N}$.

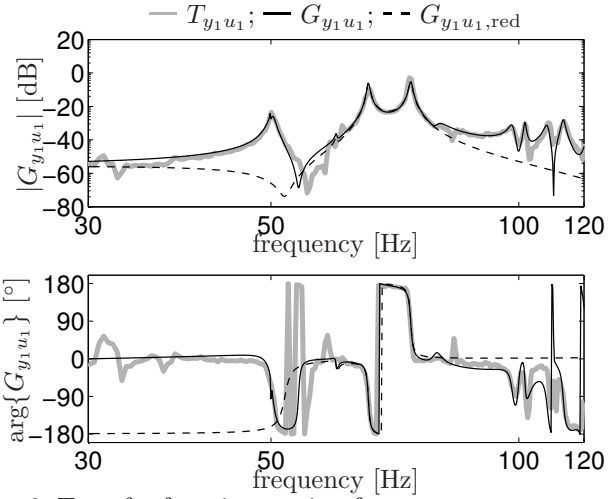


Fig. 6. Transfer function: action from $u_1$ to $y_1$

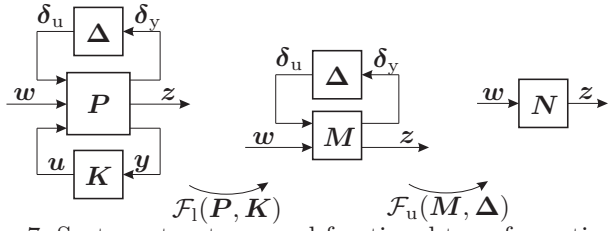


Fig. 7. System structures and fractional transformations

*5.2 Uncertainties, structured singular value, and robust stability (RS)*

Uncertainties $\boldsymbol{\Delta}$ in Fig. 7 can be any kind of parameter perturbations like uncertain natural frequencies $\omega_\mathrm{n}$ and damping coefficients $\zeta$. Additionally, an additive uncertainty $\boldsymbol{P}(s) + \boldsymbol{W}_\mathrm{a}(s)\boldsymbol{\Delta}(s)$ is utilized to model neglected high frequency dynamics. Uncertainties are assumed to be bounded by

$$||\boldsymbol{\Delta}||_\infty = \sup_{s=j\omega} \bar{\sigma}(\boldsymbol{\Delta}(s)) \leq 1, \tag{12}$$

where $\bar{\sigma}$ is the largest singular value of $\boldsymbol{\Delta}$. The structured singular value $\mu(\boldsymbol{M})$, a generalization of $\bar{\sigma}$, cannot be computed directly but can be bounded numerically by suitable inequalities (Preumont [1997]).

*5.3 Robust performance (RP)*

The aim of any control system design is not only to achieve a robustly stable system ($\mu(\boldsymbol{M}_{11}) < 1$) but also to reach the (robust) performance specification $||\mathcal{F}_\mathrm{u}(\boldsymbol{M},\boldsymbol{\Delta})||_\infty < 1$ for the closed loop system $\boldsymbol{N}$ with uncertainty $\boldsymbol{\Delta}$. A necessary and sufficient condition for RP is $\mu_{\hat{\boldsymbol{\Delta}}}(\boldsymbol{M}) < 1$, where $\hat{\boldsymbol{\Delta}} = \mathrm{diag}\{\boldsymbol{\Delta}_\mathrm{p}, \boldsymbol{\Delta}\}$, and $\boldsymbol{\Delta}_\mathrm{p}$ is a feedback uncertainty from $\boldsymbol{z}$ to $\boldsymbol{w}$.

*5.4 D-K-iteration*

An upper bound for the structured singular value of robust performance $\mu(\boldsymbol{M})$ is given by

$$\mu(\boldsymbol{M}) \leq \inf_{D\in\mathcal{D}} \bar{\sigma}(\boldsymbol{D}\boldsymbol{M}\boldsymbol{D}^{-1}). \tag{13}$$

where the scaling matrix $\boldsymbol{D}$ must satisfy $\boldsymbol{\Delta} = \boldsymbol{D}\boldsymbol{\Delta}\boldsymbol{D}^{-1}$. The synthesis procedure is therefore defined as a minimization of this upper bound over frequency:

$$\min_K(\inf_{D\in\mathcal{D}} ||\boldsymbol{D}\boldsymbol{M}\boldsymbol{D}^{-1}||_\infty). \tag{14}$$

Since the combined optimization problem (14) is not convex, a procedure known as D-K-iteration is used, which alternately keeps $\boldsymbol{D}$ fixed and optimizes for $\boldsymbol{K}$, and vice versa. A more detailed presentation is given in Benatzky et al. [2007] and an elementary introduction to robust control can be found in Preumont [1997].

## 6. CONTROLLER DESIGN

As already stated, the reduced order model $\boldsymbol{G}_\mathrm{red}$ containing only three modes is utilized for control design based on the $\mu$-synthesis methodology. An extensive treatment and comparison of controller design methods is given in Benatzky et al. [2007]. In the following, the design and performance at the scaled experimental model and later-on in co-simulations of a full-size metro car vehicle are shown.

*6.1 D-K-synthesis design*

For a realistic design additional measurement noise inputs $\boldsymbol{n}$ are fed into the identified reduced order model of the flexible structure $\boldsymbol{G}_\mathrm{red}$ (see section 4.2). With the input weight $\boldsymbol{W}_d$ for the disturbance, the remaining weights for performance are $\boldsymbol{W}_{\mathrm{p},u}$ and $\boldsymbol{W}_{\mathrm{p},a}$ (control energy and acceleration signals, respectively), the additive uncertainty is $\boldsymbol{W}_\mathrm{a}$, and the measurement noise filter is $\boldsymbol{W}_n$.

The choice of the performance weights $\boldsymbol{W}_{\mathrm{p},u}$ and $\boldsymbol{W}_{\mathrm{p},a}$ is based on a pre-scaling of the maximal singular values $\sup_\omega(\bar{\sigma})$=1 of the different transfer functions contained in $\boldsymbol{G}_\mathrm{red}$. The additive uncertainty weight $\boldsymbol{W}_\mathrm{a}$ is chosen according to Fig. 8: The uncertainty is small where the model for controller design $\boldsymbol{G}_{yu,\mathrm{red}}$ is accurate and large where no system information is contained in the model. The controller $\boldsymbol{K}_\mathrm{DK}$ is the result of the D-K-iteration

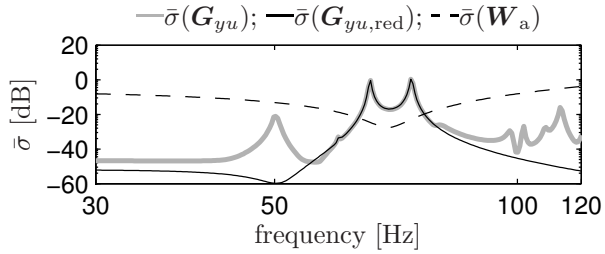


Fig. 8. Singular values $\bar{\sigma}$ of $\boldsymbol{G}_{yu}$, $\boldsymbol{G}_{yu,\mathrm{red}}$, and $\boldsymbol{W}_\mathrm{a}$

procedure, and in Fig. 9 the predicted performance enhancement using this $\boldsymbol{K}_\mathrm{DK}$ controller becomes apparent. The dashed line represents the performance of a state-feedback controller $\boldsymbol{K}_\mathrm{PP}$ using a Kalman-filter as observer (Benatzky et al. [2007]). The implementation at the scaled experiment shows that the robust controller $\boldsymbol{K}_\mathrm{DK}$ obtained by D-K-iteration achieves much better performance than $\boldsymbol{K}_\mathrm{PP}$. It is important to note that the advantage of $\boldsymbol{K}_\mathrm{DK}$ already exists for the nominal case without any uncertainties $\boldsymbol{\Delta}$.

## 7. ACTUATOR FEASIBILITY

It was shown that readily available piezo stack actuators (as specified in section 2) allow for effective vibration

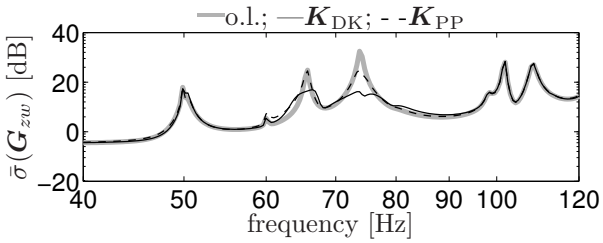


Fig. 9. Max. singular values of $\boldsymbol{G}_{zw}$ for the open (o.l.) and the closed loop case ($\boldsymbol{K}_{\mathrm{DK}}$, $\boldsymbol{K}_{\mathrm{PP}}$)

control of a full-size metro vehicle car body. Tensile forces in the actuator stacks are avoided by system design (preloaded configuration encapsulated in a robust metal shell, secured lift-off at excessive elongation). Also, temperature differences have not been found critical, as even though metro vehicles can operate in a considerable temperature span of 60°, temperature differences between car body and actuator were negligible in experiments. Furthermore, the force reference point can be appropriately set by applying an adaptive voltage offset. The setup used (see Fig. 10 for the experimental setup of a commercially available stack actuator) is highly energy efficient, using a power

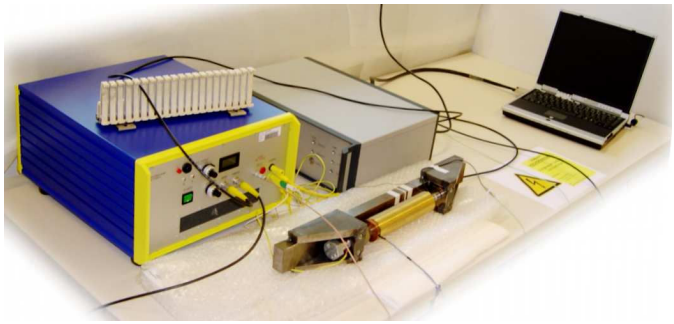

Fig. 10. Experimental setup of a piezo-stack actuator

recovering high-voltage amplifier. The net electrical power consumption of a one-actuator laboratory test bed always stayed below 150W (at 15Hz, ±1.8kN, and ±450V).

An open question is that of long-time reliability and fatigue. However, high-power cycle counts of up to $10^{10}$ are reported from the piezo actuator manufacturer, which would suffice for an actuator life-time of more than 10 years at 12h/day continuous full-stroke operation at a main working frequency of 10Hz. The use of stack actuators (instead of monolithic ones), as well as special considerations in their construction enable long lasting solutions.

## 8. CO-SIMULATION

The proposed control concept was furthermore validated in extensive co-simulation studies. Rail vehicle test runs with active vibration control were simulated in order to evaluate the controller performance at a highly realistic system behavior.

### *8.1 Modeling and implementation*

The co-simulation structure is partitioned into the control part (simulated with MATLAB/Simulink) and the multibody dynamic system simulation of the vehicle (simulated with SIMPACK). During simulation, these computations run in parallel and the SIMAT interface handles data exchange and synchronization (see Fig. 11). The rail ve-

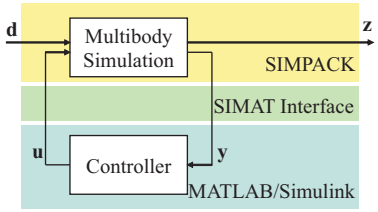


Fig. 11. Co-simulation of rail vehicle and controller

hicle is modeled in terms of elastic (car body) and rigid (bogies, wheel sets) bodies and connecting elements (including wheel-rail interaction). Two different track excitation scenarios were used in the co-simulation, entering the simulation as geometric irregularities ("Deutsche Bahn-High" and "Frederich, bad track", Frederich [1984]).

Direct acceleration measurements at nine performance positions at the vehicle floor enables ride comfort evaluation as proposed in ISO 2631 and the UIC 513 guidelines. A single ride comfort comparison value $\bar{\kappa}$ is computed by 1) weighting the nine vertical acceleration signals $a_{z,i}$ with the respective filter defined in ISO 2631, 2) calculating the RMS value over the simulation time, 3) relating each sensor's weighted RMS value to a reference weighted RMS value from a non-controlled test ride, and 4) averaging these ratios over all performance positions. The $\mu$-synthesis controller has been designed as outlined in section 6 and has been optimized for robust performance with regard to realistic actuator and sensor limitations.

### *8.2 Results*

All results are referenced to open-loop test rides of a light-weight car body vehicle; its main vibration modes are summarized in Tab. 2. Table 3 shows average ride quality

Table 2. Primary structure vibration modes of the light-weight car body

| | |
|---|---|
| Diagonal distortion mode | 7.1Hz |
| Bending mode | 8.5Hz |
| Torsion mode | 9.5Hz |

indices $\bar{\kappa}$ of a conventional (heavier and stiffer, otherwise identical) vehicle without vibration control, as well as of the light-weight vehicle using a $\mu$-synthesis controller. The control can be accomplished by four off-the-shelf piezo-stack actuators as defined in section 2. The PSD-plots

Table 3. Averaged ride quality indices $\bar{\kappa}$ for different configurations and excitations

| | Ride quality index $\bar{\kappa}$ | | |
|---|---|---|---|
| Vehicle | Conv. | Light-weight | Light-weight |
| Act. placement | (none) | Floor | Door/roof |
| 80km/h,DB-High | 0.836 | 0.796 | 0.729 |
| 100km/h,DB-High | 0.886 | 0.841 | 0.799 |
| 80km/h,Fred.bad | 0.946 | 0.722 | 0.699 |
| 100km/h,Fred.bad | 0.997 | 0.801 | 0.791 |

in Fig. 12 show that the bending and torsion modes are well damped, while the diagonal distortion mode cannot

be attenuated with this actuator configuration. It is also obvious that a higher-order mode at about 10.5 Hz is slightly excited. This vibration mode is of more complex, mixed shape with characteristics of the diagonal-distorted mode, the torsion mode and local structure deformations.

An average improvement of 20.4% (see Tab. 3) is achieved for $v = 80$ km/h at "DB-High" excitation, while the conventional vehicle without vibration control only yields 16.4% improvement in the same setting. Further studies have shown that placing actuators at vertical door columns and along roof trusses yields good controllability of all three vibration modes and results in an excellent improvement of 27.1%. However, this configuration suffers from less stiff mounting positions, which might render the use of currently available piezo-stack actuators (maximum strain $2\%_o$) complicated or infeasible.

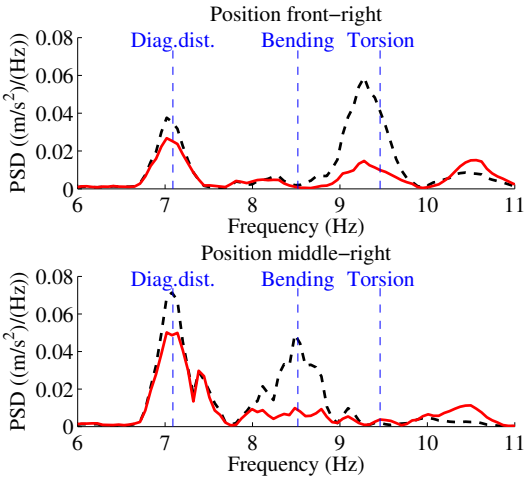


Fig. 12. Acceleration PSD-plots: Controlled test ride (4 actuators along floor trusses)(red,solid) and non-controlled reference ride (black,dashed) at $v = 80$km/h, DB-High excitation

## 9. CONCLUSION

In this paper the potential of active vibration damping has been demonstrated. Both an experimental 1/10 scaled model of a heavy metro vehicle, measurements of a full-size piezo-stack actuator, and an extensive co-simulation document the versatility and performance of the concept. The complete design steps from the FE-model to a modal state-space representation, an adequate identification procedure, and a robust controller design utilizing a $\mu$-synthesis are incorporated. The robust controller is superior to conventional control concepts, and only the D-K-design explicitly takes into account characteristics from actuator to the performance positions. Results from the co-simulation prove that an improvement in passenger comfort of 20% to 27% is possible for a heavy metro vehicle. The necessary piezo-stack actuators are already commercially available and will become even more effective with technological progress.

Several important issues could not be included although they have also been thoroughly treated: Robustness of the controller with respect to load variations, a fault detection concept, and compensation of the piezo actuators' nonlinearities using a force-feedback control. The major tasks for future investigations will be the constructive integration into a real vehicle and the investigation of fatigue due to harsh environment.

## REFERENCES

C. Benatzky and M. Kozek. Effects of local actuator action on the control of large flexible structures. In *Proceedings of the 16th IFAC World Congress*, Prague, Chech Republic, July 4–8, 2005.

C. Benatzky and M. Kozek. An identification procedure for a scaled metro vehicle - flexible structure experiment. In *European Control Conference (ECC) 2007*, Kos, Greece, July 2007.

C. Benatzky, M. Kozek, and H.P. Jörgl. Comparison of controller design methods for a scaled metro vehicle - flexible structure experiment. In *American Control Conference (ACC) 2007*, New York City, USA, July 2007.

S. Dietz. *Vibration and fatigue analysis of vehicle systems using component modes*. VDI-Verlag, Düsseldorf, 1999.

E. Foo and R. M. Goodall. Active suspension control of flexible-bodied railway vehicles using electro-hydraulic and electro-magnetic actuators. *Control Engineering Practice*, 8(5):507–518, 2000.

F. Frederich. *Die Gleislage - aus fahrzeugtechnischer Sicht*, volume 108 (12) of *Gleislauftechnik*, pages 355 – 361. Siemens Verlagsbuchhandlung, December 1984.

W. Gawronski. Actuator and sensor placement for structural testing and control. *Journal of Sound and Vibration*, 208(1):101–109, 1997.

J. Hansson, M. Takano, T. Takigami, T. Tomioka, and Y. Suzuki. Vibration suppression of railway vehicle carbody with piezoelectric elements (a study by using a scale model). *JSME International Journal Series C: Mechanical Systems, Machine Elements, and Manufacturing*, 47(2):451–456, June 2004.

T. Kamada, T. Tohtake, T. Aiba M., and Nagai. Active vibration control of the railway vehicle by smart structure concept. In S. Bruni and G. Mastinu, editors, *19th IAVSD Symposium - Poster Papers*, 2005.

M. Kozek, C. Bilik, and C. Benatzky. A pc-based flexible solution for virtual instrumentation of a multi-purpose test bed. *International Journal of Online Engineering*, 2(4), 2006.

A. Preumont. *Vibration control of active structures: an introduction*. Kluwer, 1997.

G. Schandl, P. Lugner, C. Benatzky, M. Kozek, and A. Stribersky. Comfort enhancement by an active vibration reduction system for a flexible railway car body. *Vehicle System Dynamics*, 45(9):835–847, September 2007.

A. Stribersky, H. Müller, and B. Rath. The development of an integrated suspension control technology for passenger trains. *Proceedings of the Institution of Mechanical Engineers, Part F: Journal of Rail and Rapid Transit*, 212(1):33–42, 1998.